

Direction splitting scheme for Navier-Stokes-Boussinesq system in spherical shell geometries

Aziz Takhirov^{a,*}, Roman Frolov^a, Peter Minev^a

^a*Department of Mathematical and Statistical Sciences, University of Alberta, Edmonton, AB, T6G 2G1, Canada*

Abstract

This paper introduces a second-order direction-splitting method for solving the incompressible Navier-Stokes-Boussinesq system in a spherical shell region. The equations are solved on overset Yin-Yang grids, combined with spherical coordinate transforms. This approach allows to avoid the singularities at the poles and keeps the grid size relatively uniform. The temporal second order accuracy for the Navier-Stokes step is achieved via an Artificial Compressibility (AC) scheme with bootstrapping. The spatial discretization is based on nonuniform centered differences on the Marker-And-Cell (MAC) stencil. The entire scheme is implemented in parallel using a domain decomposition iteration, and direction splitting approach for the local solves.

Keywords: Direction splitting; Finite difference method; Navier-Stokes; Artificial Compressibility; Yin-Yang grid;

2010 MSC: 65N12, 35Q30

1. Introduction

This article presents a new direction-splitting scheme for solving the incompressible Navier-Stokes-Boussinesq system:

$$\begin{aligned} \frac{\partial \mathbf{u}}{\partial t} + (\mathbf{u} \cdot \nabla) \mathbf{u} + \nabla p + \text{Pr} \Delta \mathbf{u} &= \mathbf{g} \text{Pr Ra} T \text{ in } \Omega \times (0, T_f] \\ \nabla \cdot \mathbf{u} &= 0 \text{ in } \Omega \times (0, T_f] \end{aligned} \quad (1.1)$$

$$\begin{aligned} \mathbf{u} &= \mathbf{0} \text{ on } \partial\Omega \times (0, T_f] \\ \frac{\partial T}{\partial t} + (\mathbf{u} \cdot \nabla) T - \Delta T &= 0 \text{ in } \Omega \times (0, T_f] \\ T &= 0 \text{ on } \partial\Omega \times (0, T_f] \end{aligned} \quad (1.2)$$

in a spherical shell domain that can be defined in terms of a spherical coordinate triple (r, θ, ϕ) as:

$$\Omega = \{(r, \theta, \phi) \in [R_1, R_2] \times [0, \pi] \times [0, 2\pi)\}.$$

In the above, \mathbf{g} is the unit gravity vector, and Pr, Ra are the Prandtl and Rayleigh numbers, respectively. The system (1.1) models the flow of a heat conducting fluid, under the assumption that only buoyancy

*Corresponding author

Email addresses: takhirov@ualberta.ca (Aziz Takhirov), frolov@ualberta.ca (Roman Frolov), pminev@ualberta.ca (Peter Minev)

forces are significant, while (1.2) models the advection-diffusion of heat. Even though for the most part of the discussion, we assume homogeneous Dirichlet boundary conditions on the two spherical surfaces $r = R_1, r = R_2$, the approach is applicable to other boundary conditions as well.

Many important geophysical and astrophysical problems, such as dynamos and ocean-atmospheric flows, occur in a spherical shell domain. A popular approach for numerical approximations has been to make use of the spherical transformation and solve the problem on a latitude-longitude grid. The obvious advantage of such reformulations is the simple computational domain, which allows the use of structured grids and the efficient schemes developed for them. Moreover, the grid can naturally follow the geometry of the domain, without requiring too many cells, as would possibly be in the case of a Cartesian formulation. However, the singularity of the transformation and the grid convergence near the poles have for many years been a difficulty in the development of accurate finite difference and pseudo-spectral schemes. As such, many different treatments have been proposed for dealing with them.

For example, in [1], the equations at the poles were replaced with pole equations, analogous to boundary conditions, while in [2], redefining the singular coordinates (cylindrical) was considered. Other suggested approaches include applying L'Hospital's rule [3] to singular terms and switching to Cartesian formulations about the poles [4].

On the other hand, the grid convergence has been a more serious issue. In particular, it produces a solution with uneven resolution, very small timesteps for explicit or IMEX schemes, and possibly causing convergence problems for iterative solvers. Therefore, different grid systems have been suggested in the literature that give quasi-uniform resolution and avoid the grid convergence problems. One such approach is the "cubed sphere" of [5], which is a grid that covers a spherical surface with six components corresponding to six faces of a cube. Even though, the resulting grid is quasi-uniform, it still has singularities at the corner points of the faces and it is non-orthogonal. Some of the other suggested unstructured grids include the isocahedral grid of [6] and non-orthogonal rhombahedral grid of [7].

We construct our numerical approximation on a set of two overlapping Yin-Yang grids as proposed by [8]. The two latitude-longitude grids are combined with two different spherical transforms whose axes are perpendicular to each other, cf. Fig. 1. Since both grids are structured, we can use the direction splitting approach with finite differences for the local approximations on each of them, and apply the idea of [9] to obtain a scheme that scales well on parallel computers. Other advantages of this approach are that the metric tensors are simple, the resolution is quasi-uniform, and it requires modest programming effort for extending the code from a single latitude-longitude grid. The Yin-Yang approach has been used for simulations of mantle convection [10], core collapse supernovae [11], atmospheric general circulation model [12] and visualization in spherical regions [13].

To our knowledge, the stability of the direction splitting approach has not been rigorously studied in the context a spherical coordinate system. Therefore, we prove below that it is unconditionally stable in case of a scalar heat equation, in a simply shaped domain (in terms of spherical coordinates). The case of the full

Navier-Stokes-Boussinesq system is much more involved and we cannot provide a rigorous proof at present. However, our numerical experience shows that the approach is still unconditionally stable if the advection terms are omitted and if the velocity-pressure decoupling is done via the AC method proposed in [14].

The rest of the paper is organized as follows. In the next Section, we briefly recall the definition of the Yin-Yang grid. In Sections 3 and 4, we present the numerical scheme for the advection-diffusion and Navier-Stokes equations on a Yin grid. In Section 5, we discuss the implementation details, and in Section 6 we present the numerical experiments.

2. Yin-Yang grid

In this section, we briefly recall the definition of the composite Yin-Yang grid following [8]. The grid consists of two identical overlapping latitude-longitude grids whose axes are perpendicular to each other. The Yin grid is based on a spherical transformation

$$\begin{cases} x &= r \sin \theta \cos \phi \\ y &= r \sin \theta \sin \phi \\ z &= r \cos \theta, \end{cases}$$

and covers the region

$$\Omega_1 := \left\{ (r, \theta, \phi) \in [R_1, R_2] \times \left[\frac{\pi}{4} - \varepsilon, \frac{7\pi}{4} + \varepsilon \right] \times \left[\frac{\pi}{4} - \varepsilon, \frac{3\pi}{4} + \varepsilon \right] \right\},$$

where $\varepsilon \ll 1$ is a parameter determining the overlap. The Yang grid is obtained via another spherical transformation:

$$\begin{cases} x &= -\tilde{r} \sin \tilde{\theta} \cos \tilde{\phi} \\ y &= \tilde{r} \cos \tilde{\theta} \\ z &= \tilde{r} \sin \tilde{\theta} \sin \tilde{\phi}, \end{cases}$$

such that its axes is perpendicular to the axes of the Yin transform, and covers the region

$$\Omega_2 := \left\{ (\tilde{r}, \tilde{\theta}, \tilde{\phi}) \in [R_1, R_2] \times \left[\frac{\pi}{4} - \varepsilon, \frac{7\pi}{4} + \varepsilon \right] \times \left[\frac{\pi}{4} - \varepsilon, \frac{3\pi}{4} + \varepsilon \right] \right\}.$$

The choice of the second axes should be such that the Yang grid fully covers the gap of the Yin one, and the overlapping subregions are of the same size (see Fig. 1). Otherwise, it is identical to the Yin grid modulo two rotations. The resulting Yin-Yang grids are quasiuniform, the coordinate transformations from (r, θ, ϕ) to $(\tilde{r}, \tilde{\theta}, \tilde{\phi})$ and its inverse, as well as the metric tensors on both grids are identical. As a consequence, the methods and codes developed for the standard latitude-longitude grid can be applied to both grids.

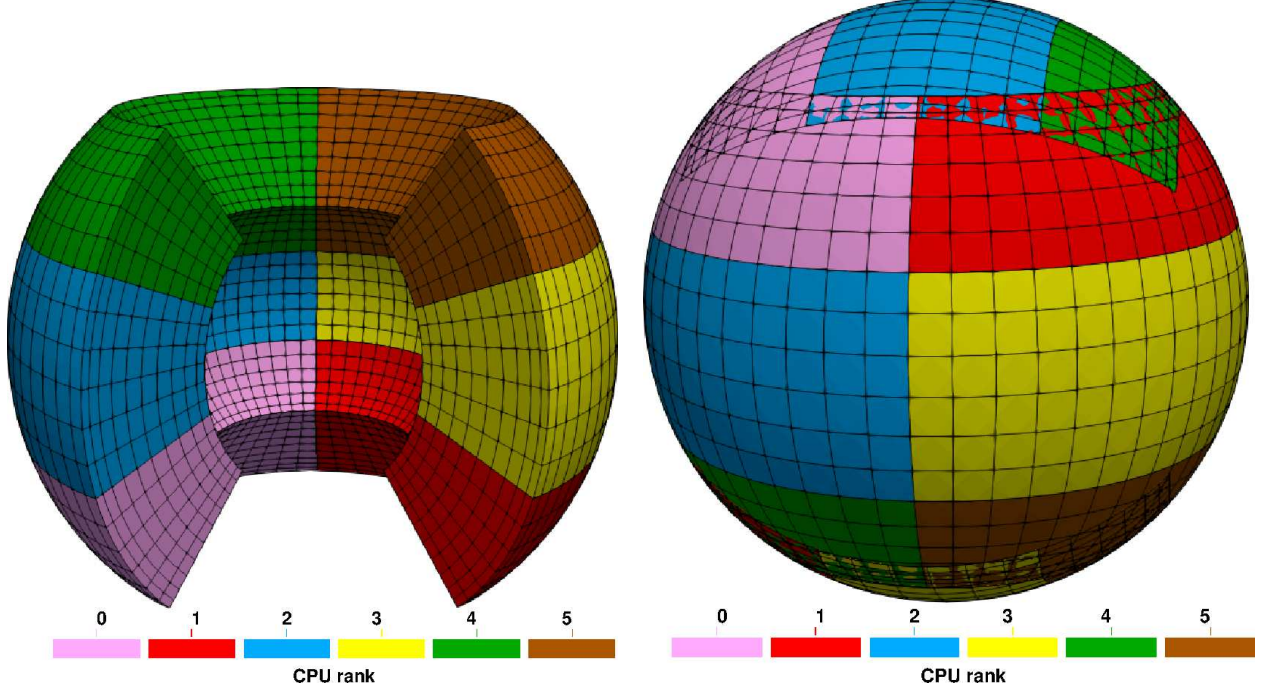


Figure 1: Yang (left) and Yin-Yang (right) grids for CPU distribution $1 \times 3 \times 2$

3. Direction-splitting discretization of the advection-diffusion equation

Since the PDEs are identical in both domains, it is sufficient to develop the numerical scheme for the Yin domain. Then the Schwarz domain decomposition method will be used to iterate between the domains.

We first present Douglas [15] type direction splitting scheme for the heat equation. Consider

$$\begin{aligned} \partial_t T - \kappa \Delta T &= 0 \text{ in } \Omega_1 \times (0, T_f], \\ T &= 0 \text{ on } \partial\Omega_1 \times (0, T_f], \end{aligned} \tag{3.1}$$

where the Laplacian in spherical coordinates is given by

$$\Delta = D_{rr} + D_{\theta\theta} + D_{\phi\phi}, D_{rr} := \frac{1}{r^2} \partial_r (r^2 \partial_r), D_{\theta\theta} := \frac{1}{r^2 \sin \theta} \partial_\theta (\sin \theta \partial_\theta), \text{ and } D_{\phi\phi} := \frac{\partial_{\phi\phi}}{r^2 \sin^2 \theta}.$$

If the spatial derivative operators are positive and commute, the stability of the direction splitting schemes is not hard to establish. However, D_{rr} , $D_{\theta\theta}$, and $D_{\phi\phi}$ do not commute with respect to the L^2 inner product:

$$(u, v) := \int_{\Omega} u v r^2 \sin \theta d\Omega.$$

To obtain a provably unconditionally stable scheme for the heat equation, we first define the following stabilized operators:

$$\hat{D}_{\theta\theta} := \frac{1}{R_1^2 \sin \theta} \partial_\theta (\sin \theta \partial_\theta), \hat{D}_{\phi\phi} := \frac{\partial_{\phi\phi}}{R_1^2 \sin^2 \theta}, \text{ and } \hat{\Delta} := D_{rr} + \hat{D}_{\theta\theta} + \hat{D}_{\phi\phi},$$

where $\theta_1 = \frac{\pi}{4} - \varepsilon$. Then it is easy to check that $D_{rr}, \hat{D}_{\theta\theta}$ and $\hat{D}_{\phi\phi}$, supplied with zero Dirichlet boundary conditions, commute. Moreover,

$$-\left(\hat{D}_{\theta\theta}T, T\right) \geq 0, \quad -\left(\hat{D}_{\phi\phi}T, T\right) \geq 0 \quad (3.2)$$

and

$$-\left(\left[\hat{D}_{\theta\theta} - D_{\theta\theta}\right]T, T\right) \geq 0 \text{ and } -\left(\left[\hat{D}_{\phi\phi} - D_{\phi\phi}\right]T, T\right) \geq 0. \quad (3.3)$$

These inequalities immediately yield that:

$$\left(-\hat{\Delta}T, T\right) \geq (-\Delta T, T). \quad (3.4)$$

Let

$$\delta T^{n+1} := T^{n+1} - T^n, T^{n+1/2} := \frac{T^{n+1} + T^n}{2} \text{ and } T^{*,n+1/2} := \frac{3T^n - T^{n-1}}{2}.$$

Denoting the timestep by τ , we propose the following direction splitting semi-discrete scheme for the (3.1):

$$\left[I - \frac{\tau}{2}D_{rr}\right] \left[I - \frac{\tau}{2}\hat{D}_{\theta\theta}\right] \left[I - \frac{\tau}{2}\hat{D}_{\phi\phi}\right] \frac{\delta T^{n+1}}{\tau} = \Delta T^{*,n+1/2} - \frac{1}{2}\hat{\Delta}\delta T^n. \quad (3.5)$$

Note that this scheme is a second-order (in time) perturbation of the second-order explicit Adams-Bashforth scheme:

$$\frac{\delta T^{n+1}}{\tau} = \Delta T^{*,n+1/2},$$

with the perturbation being given by

$$\frac{\tau^2}{2}\hat{\Delta}\frac{\delta^2 T^{n+1}}{\tau^2} + \left[\frac{\tau^2}{4}(D_{rr}\hat{D}_{\theta\theta} + D_{rr}\hat{D}_{\phi\phi} + \hat{D}_{\theta\theta}\hat{D}_{\phi\phi}) - \frac{\tau^3}{8}D_{rr}\hat{D}_{\theta\theta}\hat{D}_{\phi\phi}\right] \frac{\delta T^{n+1}}{\tau}.$$

Theorem 3.1. *The semi-discrete scheme (3.5) is unconditionally stable; more precisely, it satisfies the following estimate:*

$$\begin{aligned} \tau \sum_{n=1}^{N-1} \frac{\|T^{n+1} - T^n\|^2}{\tau^2} + \frac{1}{2}\|\nabla T^N\|^2 + \frac{1}{4}(\|\partial_\theta(T^N - T^{N-1})\|_{\omega_1}^2 + \|\partial_\phi(T^N - T^{N-1})\|_{\omega_2}^2) \\ \leq \frac{1}{2}\|\nabla T^1\|^2 + \frac{1}{4}(\|\partial_\theta(T^1 - T^0)\|_{\omega_1}^2 + \|\partial_\phi(T^1 - T^0)\|_{\omega_2}^2), \end{aligned} \quad (3.6)$$

where $\omega_1 = \left(1 - \frac{r^2}{R_1^2}\right) \sin \theta \geq 0$ and $\omega_2 = \left(\frac{r^2}{R_1^2} - 1\right) \frac{\sin \theta}{\sin^2 \theta_1} \geq 0$.

Proof 3.2. *Expanding the left hand side of (3.5) we get:*

$$\left[I - \frac{\tau}{2}\Delta + \frac{\tau^2}{4}(D_{rr}\hat{D}_{\theta\theta} + D_{rr}\hat{D}_{\phi\phi} + \hat{D}_{\theta\theta}\hat{D}_{\phi\phi}) - \frac{\tau^3}{8}D_{rr}\hat{D}_{\theta\theta}\hat{D}_{\phi\phi}\right] \frac{\delta T^{n+1}}{\tau} = \Delta T^{*,n+1/2} - \frac{1}{2}\hat{\Delta}\delta T^n. \quad (3.7)$$

Rearranging all the Δ and $\hat{\Delta}$ terms, we obtain

$$\begin{aligned} \frac{\delta T^{n+1}}{\tau} - \frac{1}{2}[\Delta - \hat{\Delta}](T^{n+1} - 2T^n + T^{n-1}) - \Delta T^{n+1/2} \\ + \left[\frac{\tau^2}{4}(D_{rr}\hat{D}_{\theta\theta} + D_{rr}\hat{D}_{\phi\phi} + \hat{D}_{\theta\theta}\hat{D}_{\phi\phi}) - \frac{\tau^3}{8}D_{rr}\hat{D}_{\theta\theta}\hat{D}_{\phi\phi}\right] \frac{\delta T^{n+1}}{\tau} = 0. \end{aligned} \quad (3.8)$$

Next we multiply (3.8) by a test function $v = \delta T^{n+1}$ and integrate by parts. Then the second term gives

$$\begin{aligned} & -\frac{1}{2} \left(\left[\Delta - \hat{\Delta} \right] (T^{n+1} - 2T^n + T^{n-1}), T^{n+1} - T^n \right) \\ &= \frac{1}{4} \left[\|\partial_\theta (T^{n+1} - T^n)\|_{\omega_1}^2 - \|\partial_\theta (T^n - T^{n-1})\|_{\omega_1}^2 + \|\partial_\theta (T^{n+1} - 2T^n + T^{n-1})\|_{\omega_1}^2 \right] \\ &+ \frac{1}{4} \left[\|\partial_\phi (T^{n+1} - T^n)\|_{\omega_2}^2 - \|\partial_\phi (T^n - T^{n-1})\|_{\omega_2}^2 + \|\partial_\phi (T^{n+1} - 2T^n + T^{n-1})\|_{\omega_2}^2 \right]. \end{aligned} \quad (3.9)$$

The third term is

$$-\left(\Delta T^{n+1/2}, T^{n+1} - T^n \right) = \frac{1}{2} \left(\|\nabla T^{n+1}\|^2 - \|\nabla T^n\|^2 \right). \quad (3.10)$$

The remaining terms are all dissipative:

$$\frac{\tau}{4} \left(D_{rr} \hat{D}_{\theta\theta} \delta T^{n+1}, \delta T^{n+1} \right) = \frac{\tau}{4} \int_{\Omega} \frac{r^2 \sin \theta}{R_1^2} |\partial_{r\theta} \delta T^{n+1}|^2, \quad (3.11)$$

$$\frac{\tau}{4} \left(D_{rr} \hat{D}_{\phi\phi} \delta T^{n+1}, \delta T^{n+1} \right) = \frac{\tau}{4} \int_{\Omega} \frac{r^2 \sin \theta}{R_1^2 \sin^2 \theta_1} |\partial_{r\phi} \delta T^{n+1}|^2, \quad (3.12)$$

$$\frac{\tau}{4} \left(\hat{D}_{\theta\theta} \hat{D}_{\phi\phi} \delta T^{n+1}, \delta T^{n+1} \right) = \frac{\tau}{4} \int_{\Omega} \frac{r^2 \sin \theta}{R_1^4 \sin^2 \theta_1} |\partial_{\theta\phi} \delta T^{n+1}|^2, \quad (3.13)$$

and

$$-\frac{\tau^2}{8} \left(D_{rr} \hat{D}_{\theta\theta} \hat{D}_{\phi\phi} \delta T^{n+1}, \delta T^{n+1} \right) = \frac{\tau^2}{8} \int_{\Omega} \frac{r^2 \sin \theta}{R_1^4 \sin^2 \theta_1} |\partial_{r\theta\phi} \delta T^{n+1}|^2. \quad (3.14)$$

Substituting (3.9)-(3.14) into (3.8), and summing for $n = 1, \dots, N-1$ completes the proof.

The factorized scheme for (1.2) is obtained in a similar fashion and takes the following form:

$$\begin{aligned} & \left[I - \frac{\tau}{2} \left(D_{rr} - u_r^{n+1/2} \partial_r \right) \right] \left[I - \frac{\tau}{2} \left(\hat{D}_{\theta\theta} - u_\theta^{n+1/2} \frac{\partial_\theta}{r} \right) \right] \left[I - \frac{\tau}{2} \left(\hat{D}_{\phi\phi} - u_\phi^{n+1/2} \frac{\partial_\phi}{r \sin \theta} \right) \right] \frac{\delta T^{n+1}}{\tau} \\ &= \Delta T^{*,n+1/2} - \frac{1}{2} \hat{\Delta} \delta T^n + \mathbf{u}^{n+1/2} \cdot \nabla T^n. \end{aligned} \quad (3.15)$$

4. Direction-splitting discretization of the Navier-Stokes system

Now we present the direction splitting scheme for the Navier-Stokes equations (1.1). Our numerical scheme is based on the AC regularization:

$$\begin{aligned} \partial_t \mathbf{u}_1 + (\mathbf{u}_1 \cdot \nabla) \mathbf{u}_1 + \nabla p_1 - \frac{1}{\text{Re}} \Delta \mathbf{u}_1 &= \mathbf{0} \\ \chi \tau \partial_t p_1 + \nabla \cdot \mathbf{u}_1 &= 0, \end{aligned} \quad (4.1)$$

where $\chi = \mathcal{O}(1)$ and Re is Reynolds number. It is well-known that the resulting approximation (\mathbf{u}_1, p_1) is first-order accurate in time (see [16]). The second order scheme can be constructed using the bootstrapping

approach of [14, 17], which requires the solution of a similar system:

$$\begin{aligned}\partial_t \mathbf{u}_2 + (\mathbf{u}_2 \cdot \nabla) \mathbf{u}_2 + \nabla p_2 - \frac{1}{\text{Re}} \Delta \mathbf{u}_2 &= \mathbf{0} \\ \chi \tau \partial_t (p_2 - p_1) + \nabla \cdot \mathbf{u}_2 &= 0\end{aligned}$$

In the following, for the sake of brevity, we will only discuss the direction splitting implementation of the first order approximation (4.1). The higher order correction for \mathbf{u}_2, p_2 is solved identically. First, consider the standard semi-implicit Crank-Nicholson approximation of the system for (\mathbf{u}_1, p_1) :

$$\begin{aligned}\frac{\mathbf{u}_1^{n+1} - \mathbf{u}_1^n}{\tau} + \mathbf{u}_2^{*,n+1/2} \cdot \nabla \mathbf{u}_1^{n+1/2} + \nabla p_1^{n+1/2} - \frac{1}{\text{Re}} \Delta \mathbf{u}_1^{n+1/2} &= \mathbf{0} \\ \chi (p_1^{n+1} - p_1^n) + \nabla \cdot \mathbf{u}_1^{n+1/2} &= 0\end{aligned}$$

Note that we use the second order velocity \mathbf{u}_2 as advecting velocity, which allows us to assemble a single linear system for both steps. We can rewrite the momentum equation by eliminating p_1^{n+1} from the first equation:

$$\begin{aligned}\frac{\mathbf{u}_1^{n+1} - \mathbf{u}_1^n}{\tau} + \mathbf{u}_2^{*,n+1/2} \cdot \nabla \mathbf{u}_1^{n+1/2} + \nabla p_1^n - \frac{1}{\text{Re}} \Delta \mathbf{u}_1^{n+1/2} - \frac{1}{2\chi} \nabla \nabla \cdot \mathbf{u}_1^{n+1/2} &= \mathbf{0} \\ p_1^{n+1} = p_1^n - \frac{1}{\chi} \nabla \cdot \mathbf{u}_1^{n+1/2}.\end{aligned}$$

In order to produce a factorized scheme for each velocity component, the $\nabla \nabla \cdot$ operator must be approximated by a sparse operator. In our implementation, we use the Gauss-Seidel type approximation of the $\nabla \nabla \cdot$ operator, which was originally proposed in [17] for Cartesian case:

$$\nabla \nabla \cdot \mathbf{u}^{n+1/2} \simeq \begin{pmatrix} \partial_r \left(\frac{\partial_r (r^2 u_r^{n+1/2})}{r^2} + \frac{\partial_\theta (\sin \theta u_\theta^{*,n+1/2})}{r \sin \theta} + \frac{\partial_\phi u_\phi^{*,n+1/2}}{r \sin \theta} \right) \\ \frac{\partial_\theta}{r} \left(\frac{\partial_r (r^2 u_r^{n+1/2})}{r^2} + \frac{\partial_\theta (\sin \theta u_\theta^{n+1/2})}{r \sin \theta} + \frac{\partial_\phi u_\phi^{*,n+1/2}}{r \sin \theta} \right) \\ \frac{\partial_\phi}{r \sin \theta} \left(\frac{\partial_r (r^2 u_r^{n+1/2})}{r^2} + \frac{\partial_\theta (\sin \theta u_\theta^{n+1/2})}{r \sin \theta} + \frac{\partial_\phi u_\phi^{n+1/2}}{r \sin \theta} \right) \end{pmatrix} := \begin{pmatrix} D_{11} & D_{12} & D_{13} \\ D_{21} & D_{22} & D_{23} \\ D_{31} & D_{32} & D_{33} \end{pmatrix} \mathbf{u}^{n+1/2}$$

60 4.1. Equation for the r -component of the velocity

Using the mass conservation equation $\nabla \cdot \mathbf{u} = 0$, it is possible to write the first component of the system as follows:

$$\partial_t u_r + \mathbf{u} \cdot \nabla u_r - \frac{\Delta u_r}{\text{Re}} + \partial_r p + \frac{1}{\text{Re}} \frac{2u_r}{r^2} - \frac{1}{\text{Re}} \frac{2}{r^3} \partial_r (u_r r^2) - \frac{u_\theta^2 + u_\phi^2}{r} = 0,$$

where $\mathbf{u} \cdot \nabla v = u_r \partial_r v + u_\theta \frac{\partial_\theta v}{r} + u_\phi \frac{\partial_\phi v}{r \sin \theta}$ is the advection operator. Let $L_{rr}, L_{r\theta}$ and $L_{r\phi}$ be the differential operators that act in each space direction:

$$L_{rr} u = \frac{1}{\text{Re}} \left(D_{rr} u - \frac{2u}{r^2} + \frac{2\partial_r (r^2 u)}{r^3} \right) + D_{11} u - u_{2,r}^{*,n+1/2} \cdot \partial_r u_r, L_{r\theta} u = \left(\frac{\hat{D}_{\theta\theta}}{\text{Re}} - u_{2,\theta}^{*,n+1/2} \cdot \frac{\partial_\theta}{r} \right) u,$$

$$L_{r\phi}u = \left(\frac{\hat{D}_{\phi\phi}}{\text{Re}} - u_{2,\phi}^{*,n+1/2} \cdot \frac{\partial_{\phi}}{r \sin \theta} \right) u \text{ and } L_r = L_{rr} + L_{r\theta} + L_{r\phi}$$

The factorized scheme for the r -component takes the following form:

$$\begin{aligned} \left[I - \frac{\tau}{2} L_{r\theta} \right] \left[I - \frac{\tau}{2} L_{r\phi} \right] \left[I - \frac{\tau}{2} L_{rr} \right] \frac{u_{1,r}^{n+1} - u_{1,r}^n}{\tau} &= L_r u_{1,r}^{*,n+1/2} + \hat{\Delta} u_{1,r}^{n-1/2} - \partial_r p_1^n + \frac{D_{12} u_{1,\theta}^{*,n+1/2} + D_{13} u_{1,\phi}^{*,n+1/2}}{2\chi} \\ &+ \frac{\left(u_{\theta}^{*,n+1/2} \right)^2 + \left(u_{\phi}^{*,n+1/2} \right)^2}{r}. \end{aligned} \quad (4.2)$$

4.2. Equation for the θ -component of the velocity

Again using $\nabla \cdot \mathbf{u} = 0$, the θ -component of the momentum equation can be expressed as:

$$\begin{aligned} \partial_t u_{\theta} + \mathbf{u} \cdot \nabla u_{\theta} - \frac{\Delta u_{\theta}}{\text{Re}} + \frac{\partial_{\theta} p}{r} + \frac{1}{\text{Re}} \frac{u_{\theta}}{r^2 \sin^2 \theta} - \frac{2 \cos \theta}{\text{Re}} \frac{\partial_{\theta} (u_{\theta} \sin \theta)}{r^2 \sin^2 \theta} - \frac{2}{\text{Re}} \frac{\partial_{\theta} u_r}{r^2} - \frac{2 \cos \theta}{\text{Re}} \frac{\partial_r (u_r r^2)}{r^3 \sin \theta} \\ + \frac{u_r u_{\phi} + u_{\theta} u_{\phi} \cot \theta}{r} = 0. \end{aligned}$$

Let $L_{\theta r}$, $L_{\theta\theta}$ and $L_{\theta\phi}$ be defined as follows:

$$\begin{aligned} L_{\theta r} u &= \left(\frac{D_{rr}}{\text{Re}} - u_{2,r}^{*,n+1/2} \cdot \partial_r \right) u, L_{\theta\phi} u = \left(\frac{\hat{D}_{\phi\phi}}{\text{Re}} - u_{2,\phi}^{*,n+1/2} \cdot \frac{\partial_{\phi}}{r \sin \theta} \right) u, \\ L_{\theta\theta} u &= \frac{1}{\text{Re}} \left(\hat{D}_{\theta\theta} u - \frac{u}{r^2 \sin^2 \theta} + \frac{2 \cos \theta}{\sin \theta} \partial_{\theta} (u \sin \theta) \right) + \frac{u \cdot u_{2,\phi}^{*,n+1/2} \cot \theta}{r} + u_{2,\theta}^{*,n+1/2} \cdot \frac{\partial_{\theta} u}{r} + \frac{D_{22} u}{2\chi}, \\ &\text{and } L_{\theta} = L_{\theta r} + L_{\theta\theta} + L_{\theta\phi} \end{aligned}$$

The factorized scheme for the θ -component takes the following form:

$$\begin{aligned} \left[I - \frac{\tau}{2} L_{\theta\phi} \right] \left[I - \frac{\tau}{2} L_{\theta r} \right] \left[I - \frac{\tau}{2} L_{\theta\theta} \right] \frac{u_{1,\theta}^{n+1} - u_{1,\theta}^n}{\tau} &= L_{\theta} u_{1,\theta}^{*,n+1/2} + \hat{\Delta} u_{1,\theta}^{n-1/2} - \frac{\partial_{\theta} p_1^n}{r} + \frac{D_{21} u_{1,r}^{*,n+1/2} + D_{23} u_{1,\phi}^{*,n+1/2}}{2\chi} \\ &+ \frac{1}{\text{Re}} \left(\frac{2}{r^2} \partial_{\theta} u_{1,r}^{n+1/2} + \frac{2 \cos \theta}{r^3 \sin \theta} \partial_r (u_{1,r}^{n+1/2} r^2) \right) \\ &- \frac{u_r^{*,n+1/2} \cdot u_{\phi}^{*,n+1/2}}{r}. \end{aligned} \quad (4.3)$$

4.3. Equation for the ϕ -component of the velocity

The ϕ -component of the momentum equation is given by:

$$\partial_t u_{\phi} + \mathbf{u} \cdot \nabla u_{\phi} + \frac{u_r u_{\phi} + u_{\theta} u_{\phi} \cot \theta}{r} - \frac{\Delta u_{\phi}}{\text{Re}} + \frac{\partial_{\phi} p}{r \sin \theta} + \frac{1}{\text{Re}} \left(\frac{u_{\phi}}{r^2 \sin^2 \theta} - \frac{2 \cos \theta}{r^2 \sin^2 \theta} \partial_{\phi} u_{\theta} - \frac{2}{r^2 \sin \theta} \partial_{\phi} u_r \right) = 0$$

Let $L_{\phi r}$, $L_{\phi\theta}$ and $L_{\phi\phi}$ be defined as follows:

$$\begin{aligned} L_{\phi r} u &= \left(\frac{D_{rr}}{\text{Re}} - u_{2,r}^{*,n+1/2} \cdot \partial_r \right) u \text{ and } L_{\phi\theta} u = \left(\frac{\hat{D}_{\theta\theta}}{\text{Re}} - u_{2,\theta}^{*,n+1/2} \cdot \frac{\partial_{\theta}}{r} \right) u \\ L_{\phi\phi} u &= \frac{1}{\text{Re}} \left(\hat{D}_{\phi\phi} - \frac{1}{r^2 \sin^2 \theta} \right) u - \frac{u_{\phi}^{*,n+1/2} \cdot u}{r \sin \theta} - \frac{u_{2,r}^{*,n+1/2} + u_{2,\theta}^{*,n+1/2} \cot \theta}{r} u \text{ and } L_{\phi} = L_{\phi r} + L_{\phi\theta} + L_{\phi\phi} \end{aligned}$$

The factorized scheme for the ϕ -component is then:

$$\begin{aligned} \left[I - \frac{\tau}{2} L_{\phi r} \right] \left[I - \frac{\tau}{2} L_{\phi\theta} \right] \left[I - \frac{\tau}{2} L_{\phi\phi} \right] \frac{u_{1,\phi}^{n+1} - u_{1,\phi}^n}{\tau} &= L_{\phi} u_{1,\phi}^{*,n+1/2} + \hat{\Delta} u_{1,\phi}^{n-1/2} \\ &- \frac{\partial_{\phi} p_1^n}{r \sin \theta} + \frac{1}{\text{Re}} \left(\frac{2}{r^2 \sin \theta} \partial_{\phi} u_{1,r}^{n+1/2} + \frac{2 \cos \theta}{r^2 \sin^2 \theta} \partial_{\phi} u_{1,\theta}^{n+1/2} \right) + D_{31} u_{1,r}^{n+1/2} + D_{32} u_{1,\theta}^{n+1/2}. \end{aligned} \quad (4.4)$$

4.4. Pressure update

$$p_1^{n+1} = p_1^{n-1} - \frac{1}{\chi} \nabla \cdot \mathbf{u}_1^{n+1/2}. \quad (4.5)$$

5. The 1D implementation and parallelization

The equations (3.15), (4.2)-(4.4) are solved as a sequence of 1D equations in each space direction. For example, solving (3.15) consists of the following steps:

$$\begin{aligned} \frac{\xi^{n+1}}{\tau} &:= \frac{1}{2} \Delta T^{*,n+1/2} - \frac{1}{2} \hat{\Delta} \delta T^n + \mathbf{u}^{n+1/2} \cdot \nabla T^n \\ \frac{\eta^{n+1}}{\tau} &:= \left[\mathbf{I} - \frac{\tau}{2} \hat{\mathbf{D}}_{\theta\theta} \right] \left[\mathbf{I} - \frac{\tau}{2} \hat{\mathbf{D}}_{\phi\phi} \right] \frac{T^{n+1} - T^n}{\tau} \Rightarrow \left[\mathbf{I} - \frac{\tau}{2} \mathbf{D}_{rr} \right] \eta^{n+1} = \xi^{n+1} \\ \frac{\zeta^{n+1}}{\tau} &:= \left[\mathbf{I} - \frac{\tau}{2} \hat{\mathbf{D}}_{\phi\phi} \right] \frac{T^{n+1} - T^n}{\tau} \Rightarrow \left[\mathbf{I} - \frac{\tau}{2} \hat{\mathbf{D}}_{\theta\theta} \right] \zeta^{n+1} = \eta^{n+1} \\ \left[\mathbf{I} - \frac{\tau}{2} \hat{\mathbf{D}}_{\phi\phi} \right] (T^{n+1} - T^n) &= \zeta^{n+1} \Rightarrow T^{n+1} = (T^{n+1} - T^n) + T^n. \end{aligned}$$

Similar strategy is applied for the Navier-Stokes approximation. Each 1D system is space approximated using second-order centered finite differences on a non-uniform grid. In order to ensure the inf-sup stability, the unknowns are approximated on a MAC grid, where the velocity components are stored at the face centers of the cells, while the scalar variables are stored at the cell centers. Moreover, it also eliminates the need for artificial pressure boundary conditions.

To solve the system on each domain in parallel we use the approach developed in [9], where we first perform Cartesian domain decomposition of both computational grids using MPI, and then solve the resulting set of tridiagonal linear systems using domain-decomposition-induced Schur complement technique. We iterate between the grids using either Additive or Multiplicative Schwarz methods.

In the Additive Schwarz implementation, we assume that the total number of CPUs is even. Then we split the global communicator into two equal parts, and assign each grid one of the communicators. In the Multiplicative Schwarz implementation, we use the global communicator to solve the problem on each grid sequentially. We precompute and store all the necessary data needed for inter-grid communication, such as the ranks of the neighbours, node numbers that must receive data and their coordinates. Since the coupling between the grids is basically 2D (recall that both transformations are identical in r direction), we use bilinear (Additive) or bi-quadratic (Multiplicative) Lagrange polynomial to interpolate the data from one grid to the other.

The overall solution procedure can be summarized as follows:

Algorithm 5.1. *Repeat till convergence in the overlap:*

For $i = 1, 2$

1) Obtain interpolated boundary values T_{bd} for $\partial\Omega_i$ from Ω_{3-i} .

- 2) Solve the temperature equation in Ω_i with using extrapolated velocity values $\mathbf{u}_2^{*,n+1/2}$.
- 3) Obtain interpolated boundary values \mathbf{u}_{bd} for $\partial\Omega_i$ from Ω_{3-i} .
- 4) Update $\mathbf{u}_{bd} := \mathbf{v}$ and solve the momentum equation in Ω_i with Dirichlet boundary conditions in θ, ϕ directions and with physical boundary conditions in the r direction.
- 5) Solve for the pressure in Ω_i .
- 6) Update the pressure values near the boundary from the other grid.

End for.

We shall additionally comment on two aspects of the above algorithm. After Step 3, we have also implemented the following Conjugate Gradient Algorithm, to ensure that there is no spurious mass flux generated through the internal (artificial) boundaries due to interpolation:

If $\left| \int_{\partial\Omega_i} \mathbf{u}_{bd} \cdot \mathbf{n} \right| \geq \text{tol}$, then minimize the functional ($\tilde{\varepsilon} \ll 1$):

$$J(\mathbf{v}) := \frac{1}{2} |\mathbf{v} - \mathbf{u}_{bd}|_{\ell^2}^2 + \frac{1}{2\tilde{\varepsilon}|\partial\Omega_i|^2} \left| \int_{\partial\Omega_i \cap \{\theta, \phi \text{ bdry}\}} \mathbf{v} \cdot \mathbf{n} + \int_{\partial\Omega_i \cap \{r \text{ bdry}\}} \mathbf{u}_{bd} \cdot \mathbf{n} \right|^2,$$

using the Conjugate Gradient Algorithm until $J(\cdot) \leq \text{tol}$.

For tests with a manufactured solution, the above Conjugate Gradient step produced nearly identical result, and has been omitted in the reported results in Section 6.

Without Step 6, in our tests we observed that the convergence rate was greatly reduced. It is well-known that in a single domain formulation of the Navier-Stokes system, pressure does not need any boundary conditions. For multi-domain formulations, many different approach have used in the literature. For example, the spectral element method of [18] uses boundary conditions only on velocity, while the pseudo-time AC finite volume method of [19] also updates the pressure values near the internal boundaries.

6. Convergence and scaling tests

6.1. Time and space convergence

Using a manufactured solution (given in Cartesian form)

$$\mathbf{u} = \cos(t) (2x^2yz, -xy^2z, -xyz^2)^T, p = \cos(t)xyz, T = 2\cos(t)x^2yz, \quad (6.1)$$

we test the convergence of the solution using both versions of the scheme. For the time convergence tests, we iterated until convergence with final time $T_f = 10$. For the space convergence tests, the time step is fixed to be $\tau = 0.0001$ and the final time is $T_f = 1$. The error graphs are presented in Figure 2, which confirm the predicted second order accuracy of the scheme.

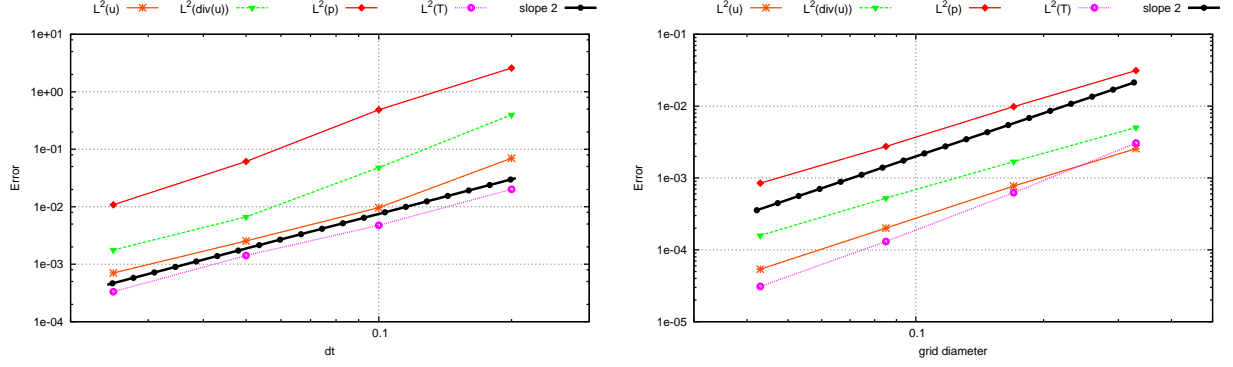


Figure 2: Log-log plot of the errors Additive Schwarz approach. Left graph contains the temporal errors at $T_f = 10$, while the right graph contains the spatial error plotted at $T_f = 1$

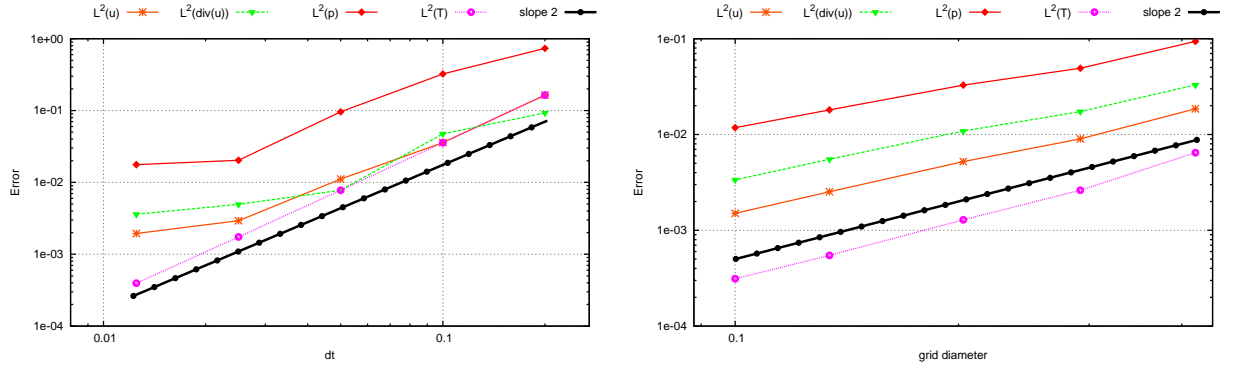


Figure 3: Log-log plot of the errors Multiplicative Schwarz approach. Left graph contains the temporal errors at $T_f = 10$, while the right graph contains the spatial error plotted at $T_f = 1$

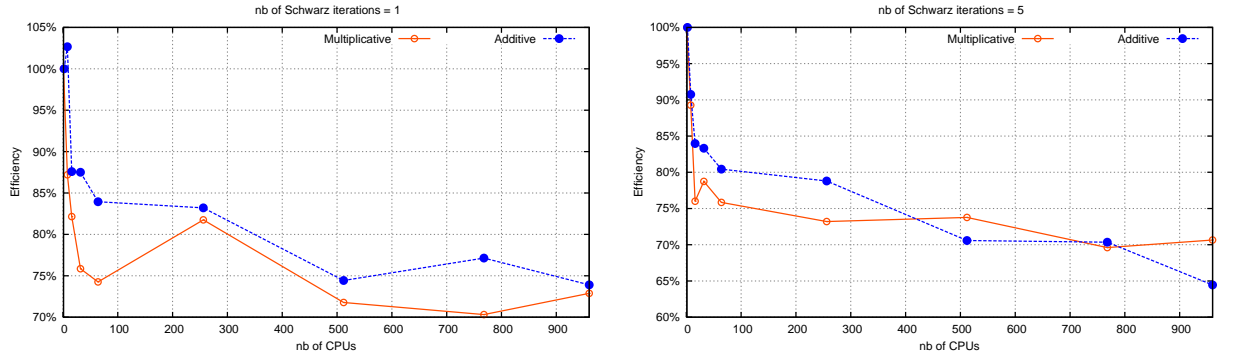


Figure 4: Parallel scalability using up to 960 CPU cores

6.2. Weak parallel efficiency

Next we test the parallel efficiency of both codes. Since we are interested in solving large size problems, we only measure the weak scalability of our codes. Scaling efficiency is computed as the ratio of the CPU-time on the minimum number of cores for the given case (one for Additive Schwartz, two for Multiplicative Schwartz) to the CPU-time on n cores. The scaling results are performed using the Compute Canada (see <https://www.computecanada.ca/>) Graham cluster of 2.1GHz Intel *E5* – 2683 v4 CPU cores, 32 cores per node, and each node connected via a 100 Gb/s network. The results were calculated using the real time taken to simulate 100 time steps, averaged over 3 independent runs. The problem size is $130 \times 130 \times 130$ grid cells per CPU and maximum number of CPUs is 960. We ran two tests, using 1 and 5 domain decomposition iterations. According to the Fig. 4, for large number of CPUs, both versions of the code have similar parallel efficiency.

Acknowledgments

The authors would like to acknowledge the support, under a Discovery Grant, of the National Science and Engineering Research Council of Canada (NSERC).

This research was enabled in part by support provided by (name of the regional partner organization) (Web address) and Compute Canada (www.computecanada.ca).

References

References

- [1] W. Huang, D. M. Sloan, [Pole condition for singular problems: The pseudospectral approximation](#), J. Comput. Phys. 107 (2) (1993) 254 – 261. doi:<https://doi.org/10.1006/jcph.1993.1141>.
URL <http://www.sciencedirect.com/science/article/pii/S0021999183711411>
- [2] K. Mohseni, T. Colonius, [Numerical treatment of polar coordinate singularities](#), J. Comput. Phys. 157 (2) (2000) 787 – 795. doi:<https://doi.org/10.1006/jcph.1999.6382>.
URL <http://www.sciencedirect.com/science/article/pii/S0021999199963829>
- [3] M. D. Griffin, E. Jones, J. D. Anderson, [A computational fluid dynamic technique valid at the centerline for non-axisymmetric flow](#), Journal of Computational Physics 30 (3) (1979) 352 – 360.
doi:[https://doi.org/10.1016/0021-9991\(79\)90120-7](https://doi.org/10.1016/0021-9991(79)90120-7).
URL <http://www.sciencedirect.com/science/article/pii/0021999179901207>
- [4] P. M. J. Freund, S. Lele, [Direct simulation of a supersonic round turbulent shear layer](#), AIAA paper (97) (1997) 0760.
URL <https://arc.aiaa.org/doi/abs/10.2514/6.1997-760>

- [5] C. Ronchi, R. Iacono, P. Paolucci, The “cubed sphere”: A new method for the solution of partial differential equations in spherical coordinates, *Journal of Computational Physics* 124 (1) (1996) 93 – 114.
doi:<https://doi.org/10.1006/jcph.1996.0047>.
URL <http://www.sciencedirect.com/science/article/pii/S0021999196900479>
- [6] J. R. Baumgardner, Three-dimensional treatment of convective flow in the earth’s mantle, *Journal of Statistical Physics* 39 (5) (1985) 501–511. doi:[10.1007/BF01008348](https://doi.org/10.1007/BF01008348).
URL <https://doi.org/10.1007/BF01008348>
- [7] S. Zhong, M. T. Zuber, L. Moresi, M. Gurnis, Role of temperature-dependent viscosity and surface plates in spherical shell convection, *Journal of Geophysical Research: Solid Earth* 105 (B5) 11063–11082.
arXiv:<https://agupubs.onlinelibrary.wiley.com/doi/pdf/10.1029/2000JB900003>,
doi:[10.1029/2000JB900003](https://doi.org/10.1029/2000JB900003).
URL <https://agupubs.onlinelibrary.wiley.com/doi/abs/10.1029/2000JB900003>
- [8] A. Kageyama, T. Sato, “Yin-Yang grid”: An overset grid in spherical geometry, *Geochemistry, Geophysics, Geosystems* 5 (9). arXiv:<https://agupubs.onlinelibrary.wiley.com/doi/pdf/10.1029/2004GC000734>,
doi:[10.1029/2004GC000734](https://doi.org/10.1029/2004GC000734).
URL <https://agupubs.onlinelibrary.wiley.com/doi/abs/10.1029/2004GC000734>
- [9] J. L. Guermond, P. D. Mineev, Start-up flow in a three-dimensional lid-driven cavity by means of a massively parallel direct numerical simulation, *International Journal for Numerical Methods in Fluids* 68 (7) 856–871.
arXiv:<https://onlinelibrary.wiley.com/doi/pdf/10.1002/flid.2583>, doi:[10.1002/flid.2583](https://doi.org/10.1002/flid.2583).
URL <https://onlinelibrary.wiley.com/doi/abs/10.1002/flid.2583>
- [10] P. J. Tackley, Modelling compressible mantle convection with large viscosity contrasts in a three-dimensional spherical shell, *Physics of the Earth and Planetary Interiors* 171 (1) (2008) 7 – 18, recent
Advances in Computational Geodynamics: Theory, Numerics and Applications.
doi:<https://doi.org/10.1016/j.pepi.2008.08.005>.
URL <http://www.sciencedirect.com/science/article/pii/S0031920108002276>
- [11] Wongwathanarat, A., Müller, E., Janka, H.-Th., Three-dimensional simulations of core-collapse supernovae: from shock breakout to maximum expansion, *A&A* 577 (2015) A48. doi:[10.1051/0004-6361/201425025](https://doi.org/10.1051/0004-6361/201425025).
URL <https://doi.org/10.1051/0004-6361/201425025>
- [12] Y. Baba, K. Takahashi, T. Sugimura, K. Goto, Dynamical core of an atmospheric general circulation model on a Yin–Yang grid, *Monthly Weather Review* 138 (10) (2010) 3988–4005. arXiv:<https://doi.org/10.1175/2010MWR3375.1>,
doi:[10.1175/2010MWR3375.1](https://doi.org/10.1175/2010MWR3375.1).
URL <https://doi.org/10.1175/2010MWR3375.1>

- [13] N. Ohno, A. Kageyama, [Visualization of spherical data by Yin–Yang grid](#), Computer Physics Communications 180 (9) (2009) 1534 – 1538. doi:<https://doi.org/10.1016/j.cpc.2009.04.008>.
 URL <http://www.sciencedirect.com/science/article/pii/S0010465509001180>
- [14] J. Guermond, P. Minev, [High-order time stepping for the incompressible Navier–Stokes equations](#), SIAM Journal on Scientific Computing 37 (6) (2015) A2656–A2681. arXiv:<https://doi.org/10.1137/140975231>, doi:10.1137/140975231.
 URL <https://doi.org/10.1137/140975231>
- [15] J. Douglas, Alternating direction methods for three space variables, Numerische Mathematik 4 (1) (1962) 41–63. doi:10.1007/BF01386295.
- [16] J. Shen, On error estimates of the penalty method for unsteady Navier-Stokes equations, SIAM J. Numer. Anal. 32 (2) (1995) 386–403.
- [17] J.-L. Guermond, P. D. Minev, High-order time stepping for the Navier-Stokes equations with minimal computational complexity, J. Comput. Appl. Math. 310 (2017) 92 – 103.
- [18] B. Merrill, Y. Peet, P. Fischer, J. Lottes, A spectrally accurate method for overlapping grid solution of incompressible Navier–Stokes equations, J. Comput. Phys. 307 (2016) 60 – 93. doi:<https://doi.org/10.1016/j.jcp.2015.11.057>.
- [19] F. S. H.S. Tang, S. Casey Jones, [An overset-grid method for 3d unsteady incompressible flows](#), J. Comput. Phys. 191 (2) (2003) 567 – 600. doi:[https://doi.org/10.1016/S0021-9991\(03\)00331-0](https://doi.org/10.1016/S0021-9991(03)00331-0).
 URL <http://www.sciencedirect.com/science/article/pii/S0021999103003310>